Materials Today: Proceedings 65 (2022) 2128–2137

Contents lists available at ScienceDirect

Materials Today: Proceedings

journal homepage: www.elsevier.com/locate/matpr

Numerical simulation of heat transfer and fluid flow around a cylinder of varying cross-section

Olalekan Adebayo Olayemi [a,*], Jekayinoluwa Temitope Olabemiwo [a], Joseph Osekhoghene Dirisu [b], Oloruntobiloba Victor Ogunwoye [a], Temidayo Samsudeen Jolayem [c], Benjamin Elochukwu Anyaegbuna [c], Tirimisiyu Abiola Olaniyan [d]

[a] Department of Aeronautics and Astronautics, Faculty of Engineering and Technology, Kwara State University, Malete, 241103, Nigeria
[b] Department of Mechanical Engineering, Faculty of Engineering and Technology, Covenant University, Otta, Ogun State 112233, Nigeria
[c] Department of Mechanical Engineering, Faculty of Engineering and Technology, University of Ilorin, Ilorin 240003, Nigeria
[d] Department of Materials Science Engineering, Faculty of Engineering and Technology, Kwara State University, Malete, 241103, Nigeria

ARTICLE INFO

Article history:
Available online 13 May 2022

Keywords:
Fluid flow
Heat transfer
Numerical simulation
Varying cross-section

ABSTRACT

The present paper discusses the effects of geometric parameters on mixed convective heat transfer and fluid flow in a lid-driven square enclosure fitted with an internal elliptical cylinder. The side walls of the enclosure were kept at a cold constant temperature and the lower horizontal wall, and the top moving wall were isolated thermally while the elliptical cylinder wall was sinusoidal heated. The dimensionless equations were solved with the aid of COMSOL Multiphysics software which relies on the finite element method. Simulations were performed for different Grashof numbers $\left(10^3 \le Gr \le 10^5\right)$, aspect ratios $(1.0 \le AR \le 3.0)$, and inclination angle of the elliptical cylinder $\left(0^{\circ} \le \phi \le 90^{\circ}\right)$. Results are presented in the form of velocity streamlines, isothermal contours, and average Nusselt number. Findings from this study show that the highest heat transfer enhancement occurred when $Gr = 10^5$. Also, for all the inclination angles and Grashof numbers considered, the more the surface of the ellipse exposed to flow, the greater the heat transfer enhancement. Finally, beyond $AR = 1.5$, inclination angle of the ellipse inhibits heat transfer enhancement.

Selection and peer-review under responsibility of the scientific committee of the International Conference on Engineering for a Sustainable World.

1. Introduction

The problem of mixed convective heat transfer finds application in several engineering fields such as cooling of microchannels, nuclear reactors, spacing heating, and the food industry [1–6]. Because of the significance of mixed convective heat transfer in engineering, a lot of researchers have investigated mixed convection in various configurations, some of which include Gangawane et al. [7] who analyzed mixed convection in a square enclosure with an inner triangular cylinder that was strategically positioned. Findings revealed that the optimum heat transfer augmentation was realized when the inner block was at the mid-position. Xiong et al. [8] numerically considered mixed convection (MHD) in a triangular cavity equipped with obstacles. Their investigation showed that a positive correlation exists between the mean Nusselt number and the Richardson number. Al-Rahed et al. [9] considered mixed convective flow in a cavity containing nanofluid, it was submitted that the thermal profile improved with increasing temperature change between the heated inner elliptical block and the bottom surface of the outer cavity (see Table 1).

Park et al. [10] explored the thermal characteristics around an inner elliptical cylinder. It was argued that Reynolds number and aspect ratio increments resulted in improvement in the value of the mean Nusselt number. In an experiment conducted by Mekroussi et al. [11] on mixed-convective fluid flow in an enclosure subjected to an undulating base surface for inclination angles ranging from 0° to 180° with a Prandtl number of 0.71, it was reported that inclination angle enhancement impacted positively on the average Nusselt number. Lee et al. [12] studied the impact of flat plate rotation on the thermal and flow profiles in a square enclosure for various Rayleigh numbers; findings from their

* Corresponding author.
E-mail address: olalekan.olayemi@kwasu.edu.ng (O. Adebayo Olayemi).

https://doi.org/10.1016/j.matpr.2022.05.010

Selection and peer-review under responsibility of the scientific committee of the International Conference on Engineering for a Sustainable World.

Nomenclature

a	Semi-major axis
AR	Aspect ratio [m]
b	Semi-minor axis [m]
g	Acceleration due to gravity [m/s^2]
Gr	Grashof number
Nu	Average Nusselt number
P	dimensional pressure [Nm^{-2}]
P	dimensionless pressure
Pr	Prandtl number
Re	Reynolds number
T	Dimensional temperature [K]
T_c	Dimensional cold wall temperature [K]
T_h	Dimensional hot wall temperature [K]
X, Y	dimensionless Cartesian coordinates
u, v	Dimensional velocity components [ms^{-1}]
U, V	dimensionless velocity components
x, y	dimensional Cartesian coordinates [m]

Greek Symbols

α	thermal diffusivity [m^2 s^{-1}]
v	kinematic Viscosity [m^2 s^{-1}]
ρ	density [kg m $^{-3}$]
φ	dimensionless temperature

investigation showed that below a Rayleigh number of 1.3×10^5, the rotor enhanced heat transfer but reduced heat transfer above the Rayleigh number of 1.3×10^5. Mamun et al [13] considered a tilted trapezoidal enclosure whose base was subjected to a constant heat flux. It was realized that the average Nusselt number was maximum at 45°inclination angle for all the Richardson numbers investigated.

Yang et al. [14] discovered that the rotation of a cylinder located in a square enclosure reduced the average Nusselt number of the configuration. Selimefendigil et al. [15] reported the mixed convective flow in a square enclosure containing nanofluid and inner cylinders undergoing rotary motion; it was concluded that locating the cylinder close to the top of the enclosure improved the thermal transportation. Karimi et al. [16] numerically analyzed the thermal and flow profiles around two cylinders housed by a square cavity and submitted that Richardson number and cylinder diameter increments improved heat transfer. Olayemi et al. [17] examined the impacts of two water-based nanofluids (Fe_3O_4 & Mn-$ZnFe_2O_4$) on heat transfer enhancement due to a stretchable rotating disk, the study demonstrated that Fe_3O_4 nanofluid showed a superior thermal conductivity compared Mn-$ZnFe_2O_4$. In a mixed convective MHD flow, Olayemi et al. [18] reported the influence of adiabatic elliptic cylinder aspect ratio, heat generation parameter, and other salient parameters on the thermal and velocity fields in the domain investigated. In another study of the natural convection of H_2O-Fe_3O_4 nanofluid flow around a cylindrical barrier, Olayemi et al. [19] reported the impacts of nanofluid volume fraction and the cylinder aspect ratio on heat transfer augmentation. Their results underpinned the ability of nanoparticles in heat transfer enhancement.

Based on the literature survey conducted, not much work has been reported in square enclosures with an elliptical cylinder positioned at various inclination angles in the cavity. The current investigation used COMSOL Multiphysics software, which relies on the finite element method, to analyze the effects of the ellipsis axes ratio (AR) ellipse inclination angle (ϕ), and Grashof number (Gr) on the heat and fluid transport dynamics around an elliptical cylinder placed in a square enclosure with a top moving wall. Other approaches that could be used to analyse fluid flow and heat transfer problems are the finite difference and the finite volume methods. Results from the current investigation find application in heat exchanger design, nuclear reactor technology, and cooling of electronic components, among others.

2. Methodology

2.1. Physical model

Fig. 1(a) represents the domain under investigation. The elliptical cylinder (with aspect ratio,$AR = \frac{a}{b}$) inside the square enclosure is exposed to a sinusoidal hot temperature $\left[T_h + sin\left(\frac{\pi x}{L}\right)\right]$. The vertical cold walls of the enclosure are exposed to a constant temperature of T_c, while the moving top wall and the bottom horizontal wall are thermally insulated. Also, Fig. 1(b) depicts the mesh of the domain used for the simulation.

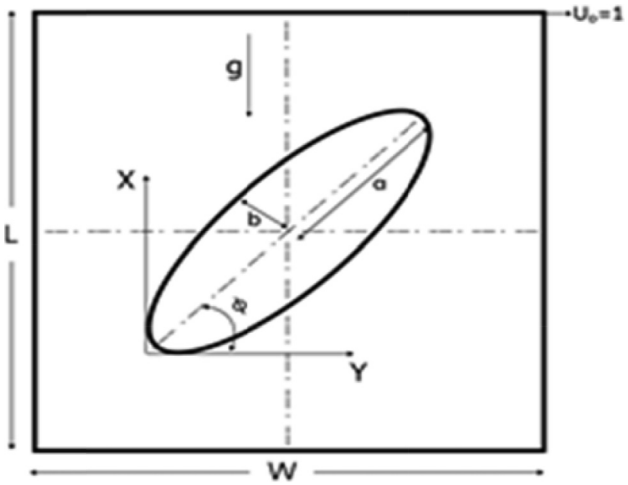

Fig. 1a. Physical geometry.

Table 1
Comparison of mean Nusselt number of the hot horizontal top boundary of the enclosure in the current study with historical data [21–23].

Re	Scheme	Grid	Gr 10^2	10^4	10^5
400	Iwatsu et al [21]	128 × 128	3.84	3.62	1.22
	Sharif [22]	100 × 100	4.05	3.82	1.17
	T.S. Cheng [23]	128 × 128	4.14	3.90	1.21
	Present	128 × 128	3.99	3.76	1.15

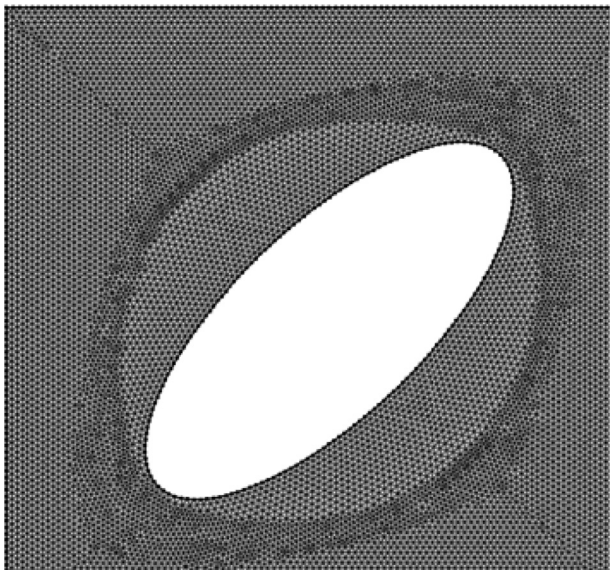

Fig. 1b. Mesh distribution.

2.2. Governing equations

The physics of the configuration being considered is described by the steady-state dimensionless Eqs. (1)–(4) stated below. The density variation in the buoyancy term in the flow equation is captured by using the Boussinesq model, and the fluid velocity in the cavity is very much less than the speed of sound. The fluid flow is assumed to be laminar and Newtonian and the fluids in contact with solid boundaries have zero velocity.

The dimensionless continuity, momentum ($\boldsymbol{X}$&$\boldsymbol{Y}$) and energy equations are given by Eqs. (1)–(4) [20]:

$$\frac{\partial U}{\partial X}+\frac{\partial V}{\partial Y}=0 \tag{1}$$

$$U\frac{\partial U}{\partial X}+V\frac{\partial U}{\partial Y}=-\frac{\partial P}{\partial X}+\frac{1}{Re}\left[\frac{\partial^2 U}{\partial X^2}+\frac{\partial^2 U}{\partial Y^2}\right] \tag{2}$$

$$U\frac{\partial V}{\partial X}+V\frac{\partial V}{\partial Y}=-\frac{\partial P}{\partial Y}+\frac{1}{Re}\left[\frac{\partial^2 V}{\partial X^2}+\frac{\partial^2 V}{\partial Y^2}\right]+\frac{Gr}{Re^2}\Theta \tag{3}$$

$$U\frac{\partial \Theta}{\partial X}+V\frac{\partial \Theta}{\partial Y}=\frac{1}{Re.Pr}\left[\frac{\partial^2 \Theta}{\partial X^2}+\frac{\partial^2 \Theta}{\partial Y^2}\right] \tag{4}$$

2.3. Normalization parameters

The dimensionless variables are expressed by Eq. (5):

$$\boldsymbol{X}=\frac{\boldsymbol{x}}{\boldsymbol{L}},\ \boldsymbol{Y}=\frac{\boldsymbol{y}}{\boldsymbol{L}},\ \boldsymbol{U}=\frac{\boldsymbol{u}}{\boldsymbol{U_0}},\ \boldsymbol{V}=\frac{\boldsymbol{v}}{\boldsymbol{U_0}},\ \Theta=\frac{\boldsymbol{T}-\boldsymbol{T_c}}{\boldsymbol{T_h}-\boldsymbol{T_c}},\ \boldsymbol{P}=\frac{\boldsymbol{p}}{\boldsymbol{\rho U_0^2}},\ \boldsymbol{Pr}=\frac{\boldsymbol{\upsilon}}{\boldsymbol{\alpha}} \tag{5}$$

The average heat transfer on the solid boundaries of the model is given by Eq. (6).

$$\bar{Nu}=\frac{1}{L}\int_0^L\frac{\partial\Theta}{\partial X}dY \tag{6}$$

3. Procedure for computation

The mesh in Fig. 1(b) which was used for the analysis of the domain under investigation was produced with the free triangular mesh in conjunction with the extremely fine mesh options in COMSOL Multiphysics software (version 5.5). The dimensionless transport equations together with the associated boundary conditions were then solved with the software. To ensure enhanced thermal and flow field resolutions, the extremely fine mesh-size option in COMSOL Multiphysics was employed as the choice for the grid-size.

4. Results

4.1. Results validation

The validation of the code used for the current investigation has been effected by comparing the mean Nusselt number obtained in the present analysis with historical data of [21–23] and the comparison shows good agreement.

Fig. 2 presents the plots of the isothermal contours and velocity streamlines for various *Gr* while maintaining ϕ = 0° and *AR* = 2.5. With increasing *Gr*, the effect of heating becomes noticeable with the formation of plumes towards the upper wall of the enclosure. The streamline plots show the formation of four vortices around the ellipse and, the flow is almost symmetric about the mid-vertical position with vigorous flow activity around the upper wall area of the enclosure which is an indication of improved heating.

Fig. 3 displays the isothermal contours and velocity streamlines for different *Gr* values when ϕ = 45° and *AR* = 2.5. The isothermal contours are like those in Fig. 2. For $Gr = 10^3$, the isothermal contours close to the vertical walls were observed to be almost parallel to the vertical walls which is an indication of a conduction dominant heat transfer regime. As *Gr* improves, the isothermal contours close to the side walls of the enclosure begin to deviate from their previous orientation which is an indication that convection had become more pronounced. At $Gr = 10^5$, the isothermal contour around the vertical walls of the enclosure becomes colder which signifies a higher delta $T\,(\Delta T)$ value and therefore, more heat transfer rate ensured. Furthermore, the velocity streamlines indicate that the fluid velocities are more vigorous around the top left and bottom right corners of the enclosure and the velocities at these locations increase with increasing *Gr*. Similarly, the velocities of the contours around the bottom corners of the enclosure also increase gradually in strength with *Gr* increment.

Fig. 4 depicts the isothermal contours and the velocity streamlines for Grashof number values of 10^3, 10^4 and 10^5 for ϕ = 90° and *AR* = 2.5. The response of the isothermal contours to Grashof number increment is similar to those of Figs. 2 and 3. However, with Grashof number improvement, the flow in the square cavity becomes predominantly limited to the left side of the ellipse. For $Gr = 10^3$, the flow in the cavity is nearly symmetric around the elliptical cylinder; when $Gr = 10^4$, two inner vortices were formed which combined to form a single vortex when $Gr = 10^5$.

Fig. 5 displays the isothermal contours and velocity streamlines for different aspect ratios when $Gr = 10^5$, and ϕ = 0°. Growth in the aspect ratio of the elliptical cylinder increases the heating of the fluid in the cavity, this is evident in the behaviour of the isothermal contours and therefore, convection becomes more pronounced, and hence more heat is transferred. For the velocity streamline plots, at *AR* = 1, the streamlines are less dense at the bottom with two secondary vortices. At *AR* = 1.5, the density of the contours increases, and each secondary vortex splits to form two vortices. Beyond *AR* of 1.0, four circulations were formed which became more distinct as *AR* increases.

Fig. 6 presents the isothermal contours and velocity streamlines for various inclination angles of the elliptical cylinder when *AR* = 2.5 and $Gr = 10^5$. As the orientation angle increases, the distribution of the isothermal contours is seen to depend largely on the

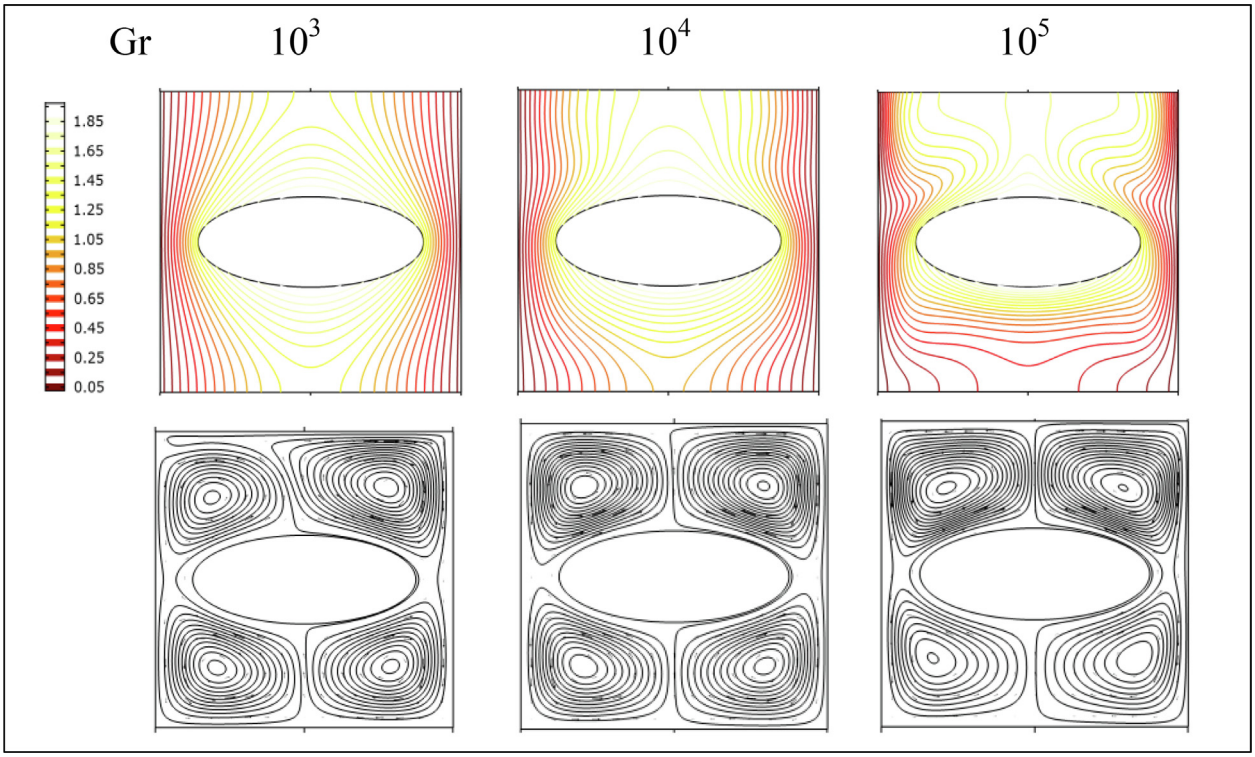

Fig. 2. The effect of Grashof number (*Gr*) on isothermal contours and streamlines when *Re* = 1, ϕ = 0° and *AR* = 2.5.

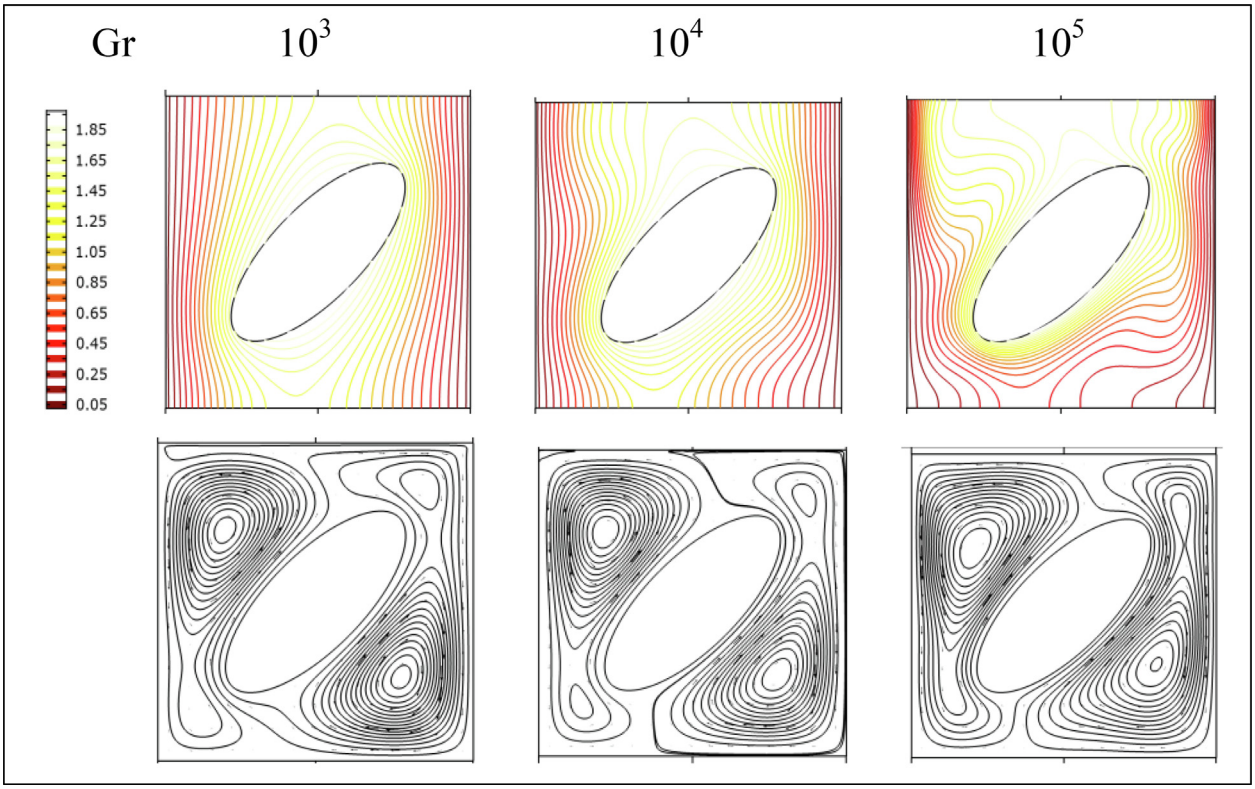

Fig. 3. The effect of Grashof number (*Gr*) on isothermal contours and streamlines when *Re* = 1, ϕ = 45° and *AR* = 2.5.

location of the ellipse. For the velocity streamlines, the top region of the enclosure is denser than beneath the elliptical enclosure. For an elliptical cylinder orientation of 15°, the streamlines became less dense especially to the right of the elliptical cylinder.

At 30° orientation, more pressure was being experienced around the lower right side of the enclosure resulting in the enlargement of the streamlines in the direction of the lower right part of the enclosure.

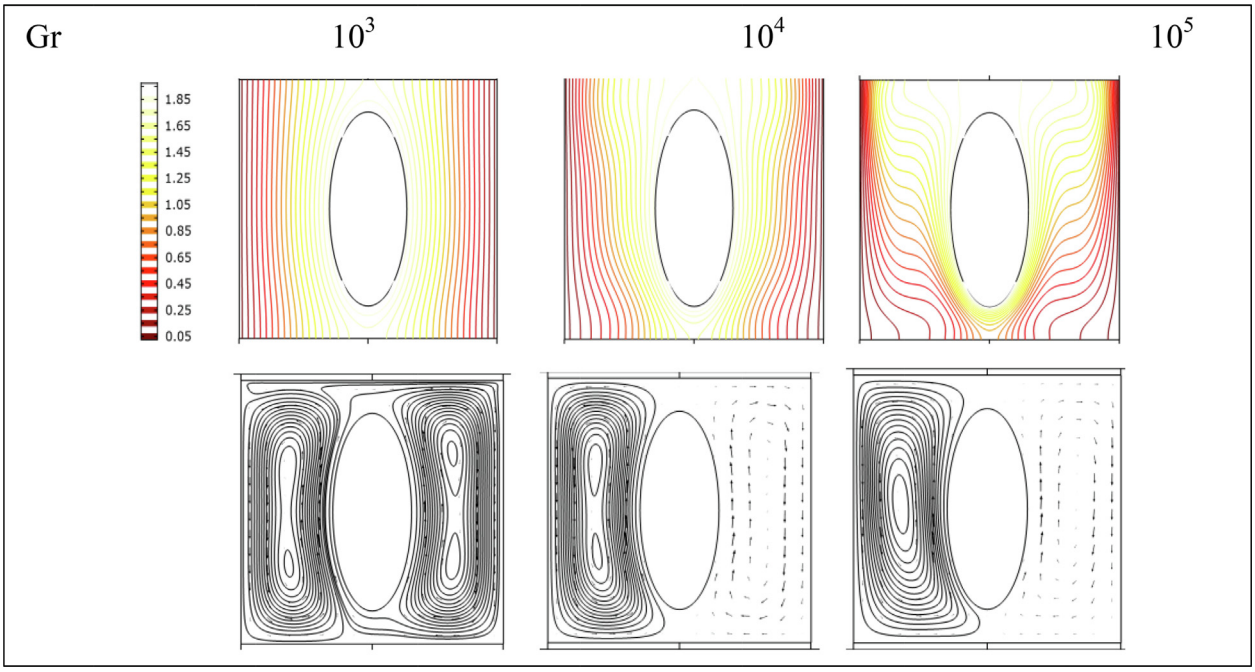

Fig. 4. The effect of Grashof number (Gr) on isothermal contours and streamlines when Re = 1, ϕ = 90° and AR = 2.5.

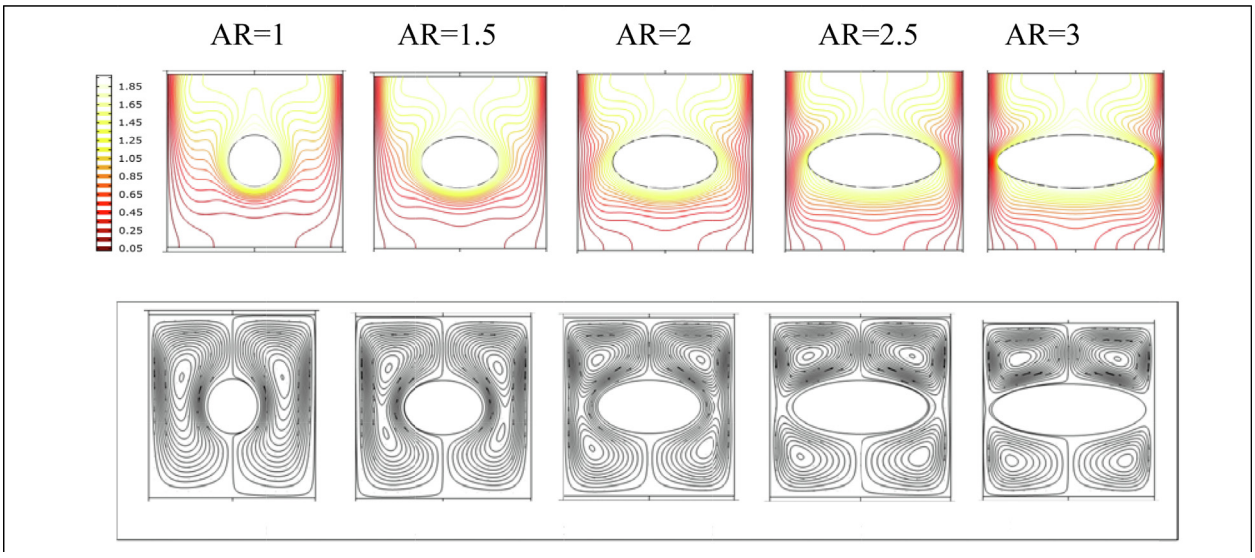

Fig. 5. The effects of Aspect Ratio (AR) on isothermal contours (upper) and velocity streamlines (lower) at Gr = 10^5, and ϕ = 0°.

Fig. 5. Plots for the isothermal contours and velocity streamline for various aspect ratios at Gr = 10^5, and ϕ = 0°.

Furthermore, on the left side, the streamlines became denser at the top and reduced at the bottom. At 45°, the vortex on the lower left bottom side disappeared as that on the top right was at the verge of vanishing. The streamlines were observed to be denser at 60° and the two vortices on both sides of the ellipse at 30° orientation had combined to form a single vortex each. From AR = 2.5 and inclination angle beyond 60°, the velocity streamlines became limited to one of the sides of the elliptical cylinder. At 75°, the streamlines on the left side of the cavity disappeared while those on the right became denser. At 90° elliptical orientation, the streamlines disappeared on the right portion of the enclosure and reappeared on the left side. This occurrence could be because the vortex strength was not able to overcome the force of gravity as elliptical cylinder tends towards 90° orientation and hence a shift in the position of the vortices.

Fig. 7 displays the velocity magnitude of the fluid flow distribution at the mid-way between the upper horizontal wall of the square enclosure and the top wall of the elliptical cylinder when AR = 3.0, Gr = 10^5, and ϕ = 0°. The plot reveals that at 5% and 95% of the enclosure wall length, the fluid attained its maximum velocity magnitude of 70. This region of maximum velocity of flow is attested to by Fig. 5 when AR = 3.0, and Fig. 6. Fig. 8 is the temperature profile plot at the mid-way between the upper horizontal

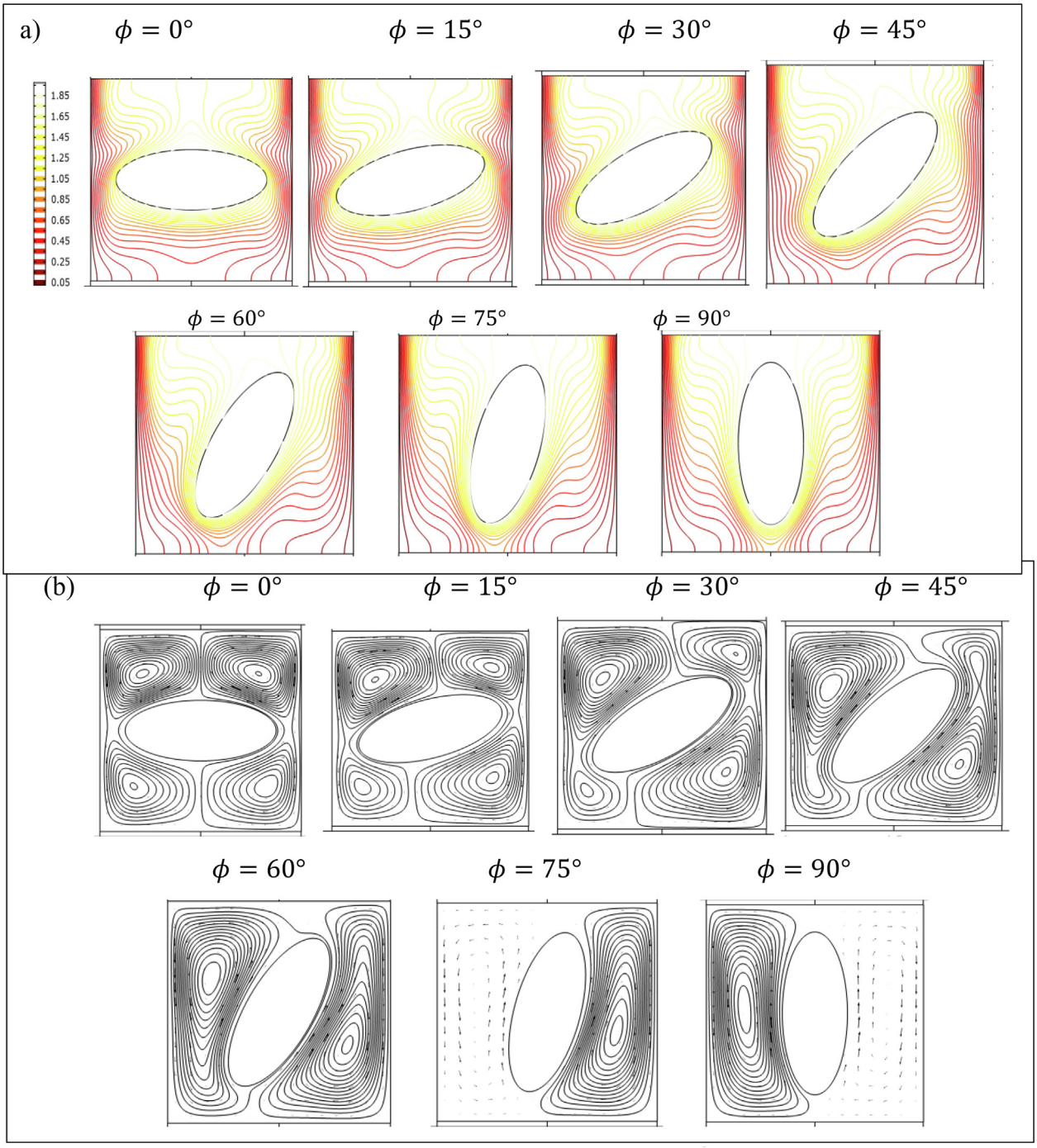

Fig. 6. The effects of Inclination angle (ϕ) on isothermlines (a) and stream function (b) at $Gr = 10^5$, and $AR = 2.5$.

wall of the square enclosure and the top wall of the elliptical cylinder when $AR = 3.0$, $Gr = 10^5$, and $\phi = 0°$. The plot shows that the maximum temperature in the enclosure is 1.73 units and it occurred at 50% of the enclosure wall length.

Figs. 9, 10, and 11 present the implication of aspect ratio on the average Nusselt number at the elliptical cylinder walls for different Gr values when $\phi = 0°$, 45° and 90°. Apparently, Gr rise results in average Nusselt number improvement, this is due to the increase in the surface area over which heat transfer occurred. This pattern of heat transfer is sustained for the various inclination angles investigated. Figs. 12 and 13 present the plots of average Nusselt number against orientation angle at the elliptical cylinder wall for various aspect ratios when $Gr = 10^3$ and 10^4 respectively. The plots in Figs. 12 and 13 show that the average Nusselt number for $AR = 1$ and 1.5 are almost insensitive to the orientation of the elliptical cylinder; also, for aspect ratio in the range of $1.5 \leq AR \leq 3$, the average Nusselt number of the elliptical cylinder decreases significantly with increasing inclination angle.

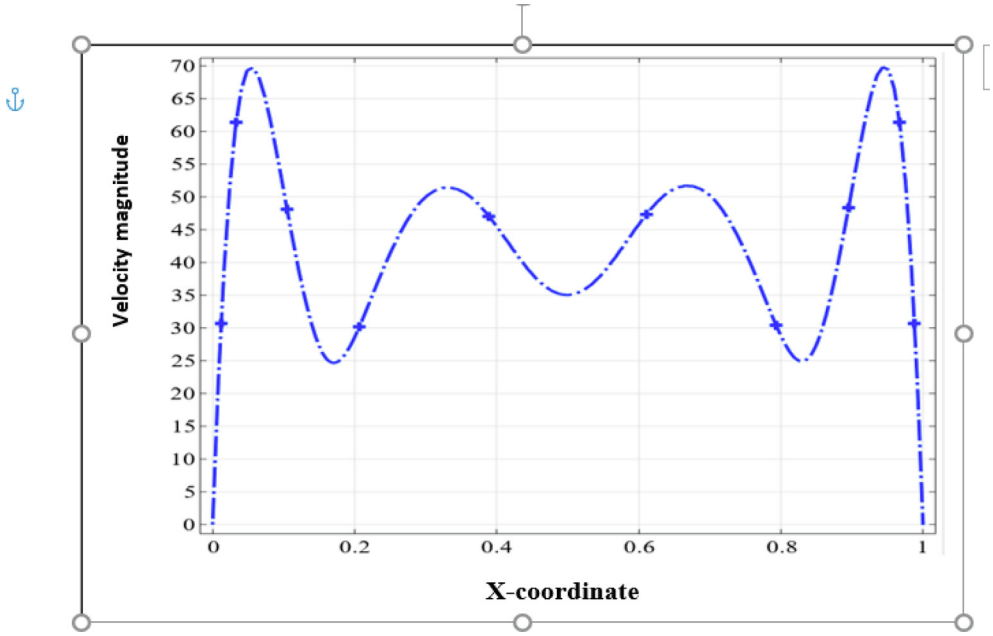

Fig. 7. Velocity magnitude at mid-plane between the upper wall of the enclosure and the top wall of the elliptical cylinder when AR = 3.0, Gr = 10^5, and ϕ = 0°.

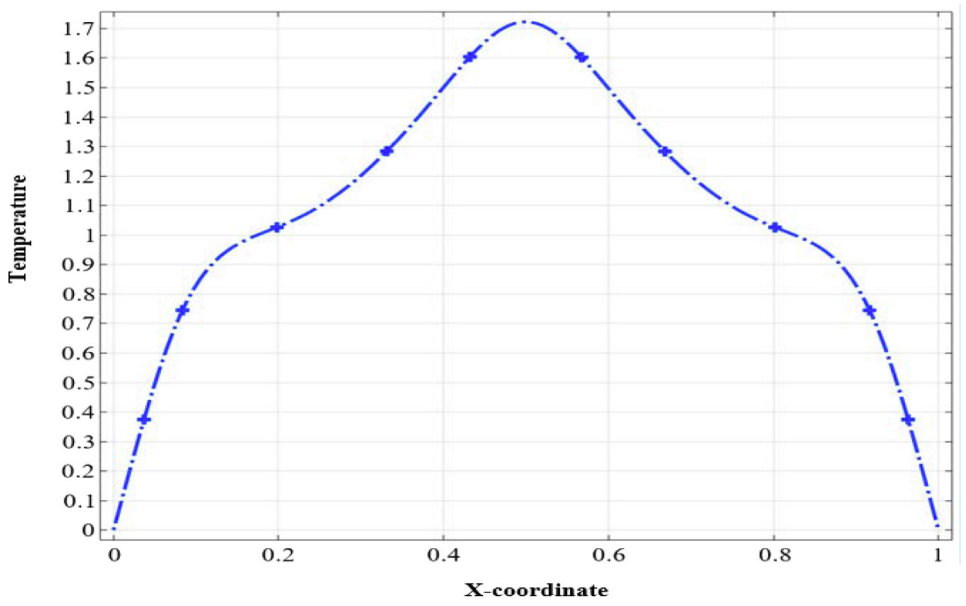

Fig. 8. Temperature profile at mid-plane between the upper wall of the enclosure and the top wall of the elliptical cylinder when AR = 3.0, Gr = 10^5, and ϕ = 0°.

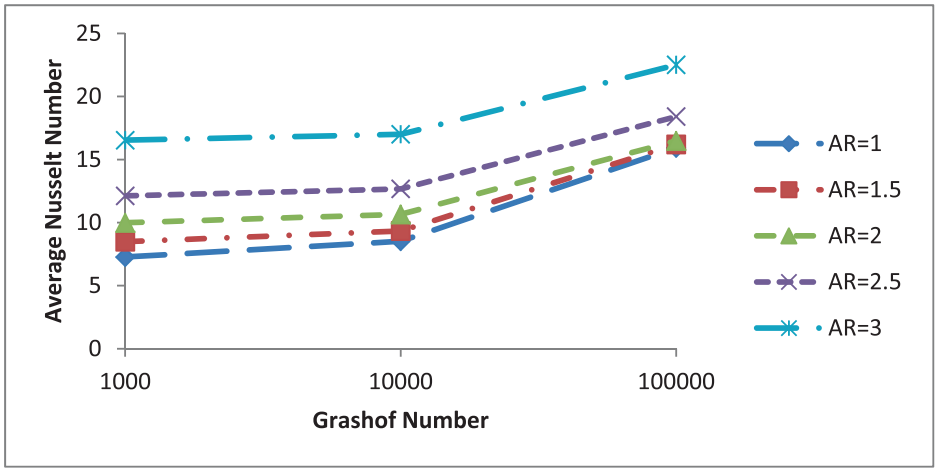

Fig. 9. Average Nusselt number versus Grashof number at the elliptical cylinder wall for several aspect ratios when in ϕ = 0°.

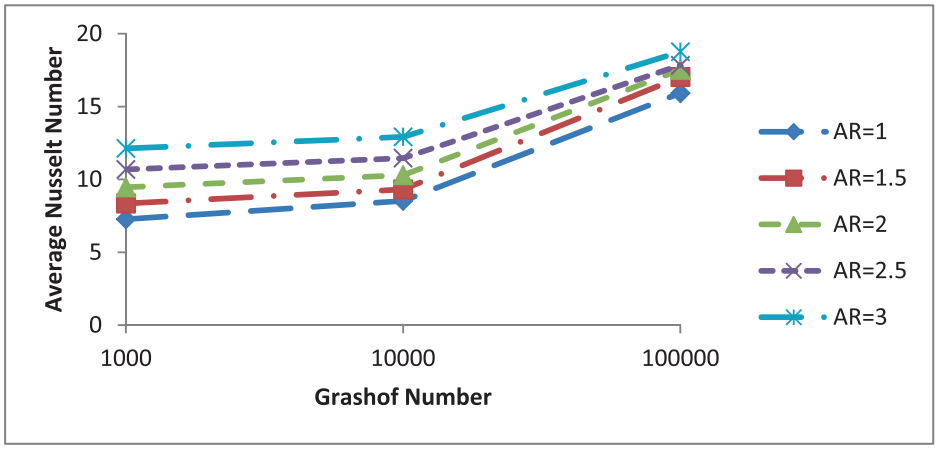

Fig. 10. Average Nusselt number versus Grashof number at the elliptical cylinder wall for several aspect ratios when in ϕ = 45°.

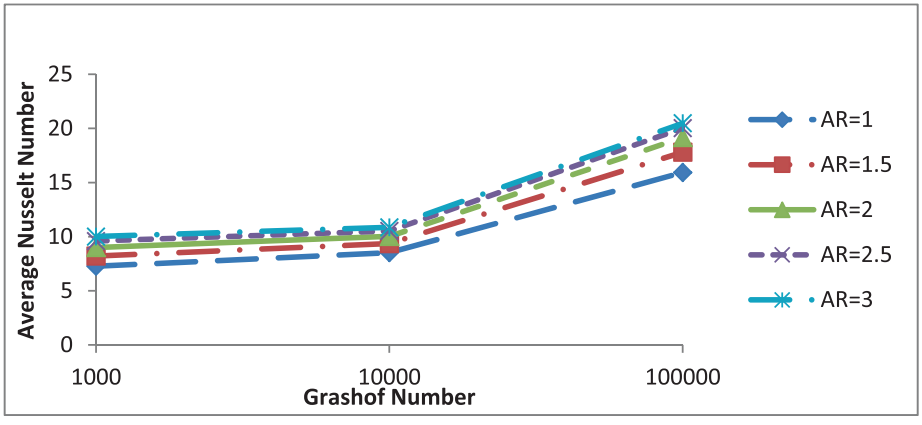

Fig. 11. Average Nusselt number versus Grashof number at the elliptical cylinder wall for several aspect ratios when in ϕ = 90°.

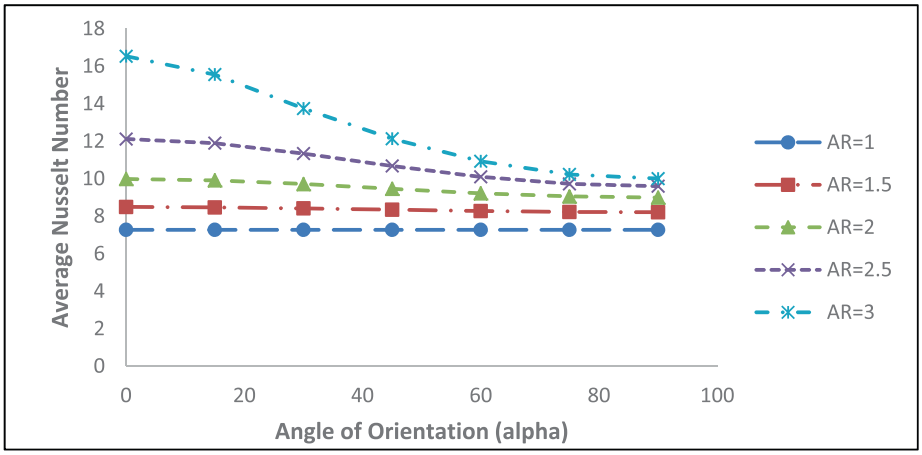

Fig. 12. Average Nusselt number of the elliptical cylinder against angle of orientation when Gr = 1E3.

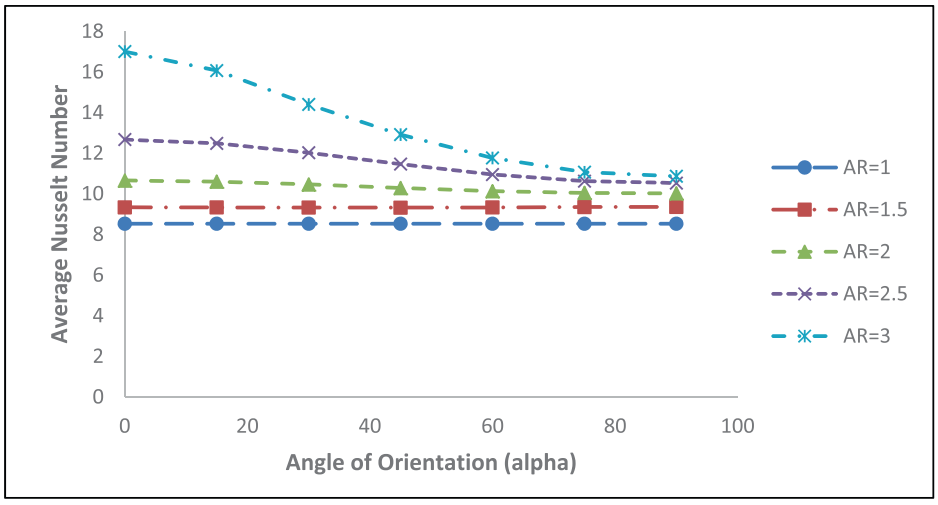

Fig. 13. Average Nusselt number of the elliptical cylinder against angle of orientation when Gr = 1E4.

5. Conclusion

The summary of the research findings is as follows:

For the range of Grashof number ($10^3 \leq Gr \leq 10^5$) and inclination angle ($0° \leq \phi \leq 90^{\circ}$) considered, aspect ratio (AR) and Grashof number (Gr) increments resulted in heat transfer augmentation at the elliptical cylinder wall. The highest heat transfer enhancement occurred when the cylinder is in a horizontal position ($i.e., \phi = 0$), $AR = 3.0$, and $Gr = 10^5$. For aspect ratio greater than 1.5, elliptical cylinder inclination discourages heat transfer enhancement. Finally, in the plane above the cylinder wall, where the heat transferred is maximum, the highest value of the velocity magnitude is 70 while the maximum dimensionless temperature at this plane is 1.72.

Declaration of Competing Interest

The authors declare that they have no known competing financial interests or personal relationships that could have appeared to influence the work reported in this paper.

References

[1] O.A. Olayemi, K. Al-Farhany, O. Olaogun, M.O. Ibiwoye, R.O. Medupin, A. Jinadu, Computational Fluid Dynamics Analysis of Mixed Convection Heat Transfer and Fluid Flow in a Lid-driven Square Cavity Subjected to Different Heating Conditions, IOP Conf. Series: Mater. Sci. Eng. 1107 (1) (2021) 012201.

[2] M.A. Alomari, K. Al-Farhany, A.L. Hashem, M.F. Al-Dawody, F. Redouane, O.A. Olayemi, Numerical Study of MHD Natural Convection in Trapezoidal Enclosure Filled With (50% MgO-50% Ag/Water) Hybrid Nanofluid: Heated Sinusoidal from Below, Int. J. Heat Technol. 39 (4) (2021) 1271–1279.

[3] O.A. Olayemi, A.F. Khaled, O.J. Temitope, O.O. Victor, C.B. Odetunde, I.K. Adegun, Parametric study of natural convection heat transfer from an inclined rectangular cylinder embedded in a square enclosure, Aust. J. Mech. Eng. 1–14 (2021).

[4] O.A. Olayemi, J.T. Olabemiwo, T.S. Jolayemi, K.O. Oladosu, C. Odetunde, I.K. Adegun, Computational Fluid Dynamics (CFD) Analysis of Buoyancy Flow in A Differentially Heated Square Cavity, IOP Conf. Series: Mater. Sci. Eng. 1107 (1) (2021) 012120.

[5] I.K. Adegun, O.A. Olayemi, T.S. Jolayemi, O.T. Ogunbodede, Laminar Forced Convective Heat Transfer and Fluid Flow in a Finned Cylindrical Annulus, FUOYE J. Eng. Technol. 2 (1) (2017) 51–58.

[6] I.K. Adegun, T.S. Jolayemi, O.A. Olayemi, A.M. Adebisi, Numerical simulation of forced convective heat transfer in inclined elliptic ducts with multiple internal longitudinal fins, Alex. Eng. J. 57 (4) (2018) 2485–2496.

[7] K.M. Gangawane, H.F. Oztop, M.E. Ali, Mixed convection in a lid-driven cavity containing triangular block with constant heat flux: Effect of location of block, Int. J. Mech. Sci. 152 (2019) 492–511.

[8] P.Y. Xiong, A. Hamid, K. Iqbal, M. Irfan, M. Khan, Numerical simulation of mixed convection flow and heat transfer in the lid-driven triangular cavity with different obstacle configurations, Int. Commun. Heat Mass Transf. 123 (2021) 105202.
[9] A.A. Al-Rashed, A. Shahsavar, M. Akbari, D. Toghraie, M. Akbari, M. Afrand, Finite Volume Simulation of mixed convection in an inclined lid-driven cavity filled with nanofluids: Effects of a hot elliptical centric cylinder, cavity angle and volume fraction of nanoparticles, Physica A Stat. Mech. Appl. 527 (2019) 121122.
[10] Y.G. Park, H.W. Cho, G.S. Mun, M.Y. Ha, Effect of the aspect ratio of an elliptical cylinder on mixed convective heat transfer within a lid-driven enclosure, J. Mech. Sci. Technol. 34 (7) (2020) 3057–3068.
[11] S. Mekroussi, D. Nehari, M. Bouzit, N.-E. Chemloul, Analysis of mixed convection in an inclined lid-driven cavity with a wavy wall, J. Mech. Sci. Technol. 27 (7) (2013) 2181–2190.
[12] S.-L. Lee, J.-B. Chiou, G.-S. Cyue, Mixed convection in a square enclosure with a rotating flat plate, Int. J. Heat Mass Transf. 131 (2019) 807–814.
[13] M.A.H. Mamun, T.R. Tanim, M.M. Rahman, R. Saidur, S. Nagata, Analysis of Mixed Convection in a Lid Driven Trapezoidal Cavity, Convect. Conduct. Heat Transf. (2011) 55–82.
[14] H. Yang, W. Zhang, Z. Zhu, Unsteady mixed convection in a square enclosure with an inner cylinder rotating in a bi-directional and time-periodic mode, Int. J. Heat Mass Transf. 136 (2019) 563–580.
[15] F. Selimefendigil, M.A. Ismael, A.J. Chamkha, Mixed convection in superposed nanofluid and porous layers in a square enclosure with inner rotating cylinder, Int. J. Mech. Sci. 124 (2017) 95–108.
[16] F. Karimi, H. Xu, Z. Wang, M.o. Yang, Y. Zhang, Numerical simulation of steady mixed convection around two heated circular cylinders in a square enclosure, Heat Transf. Eng. 37 (1) (2016) 64–75.
[17] O.A. Olayemi, A.M. Obalalu, C.B. Odetunde, O.A. Ajala, Heat transfer enhancement of magnetized nanofluid flow due to a stretchable rotating disk with variable thermophysical properties effects, Eur. Phys. J. Plus 137 (3) (2022) 1–12.
[18] O.A. Olayemi, K. Al-Farhany, A.M. Obalalu, T.F. Ajide, K.R. Adebayo, Magnetoconvection around an elliptic cylinder placed in a lid-driven square enclosure subjected to internal heat generation or absorption, Heat Transf. (2022) 1–27.
[19] O.A. Olayemi, A. Salaudeen, K. Al-Farhany, R.O. Medupin, I.K. Adgun, Modelling of heat transfer characteristics around a cylindrical barrier, Int. J. Eng. Model. 35 (1) (2022) 83–106.
[20] K. Khanafer, S.M. Aithal, Laminar mixed convection flow and heat transfer characteristics in a lid driven cavity with a circular cylinder, Int. J. Heat Mass Transf. 66 (2013) 200–209.
[21] R. Iwatsu, J.M. Hyun, K. Kuwahara, Mixed convection in a driven cavity with a stable vertical temperature gradient, Int. J. Heat Mass Transf. 36 (6) (1993) 1601–1608.
[22] M.A.R. Sharif, Laminar mixed convection in shallow inclined driven cavities with hot moving lid on top and cooled from bottom, Appl. Therm. Eng. 27 (5-6) (2007) 1036–1042.
[23] T.S. Cheng, Characteristics of mixed convection heat transfer in a lid-driven square cavity with various Richardson and Prandtl numbers, Int. J. Therm. Sci. 50 (2) (2011) 197–205.